Regression models and intensity measure pairs for offshore wind turbine multi-hazard fragility functions

Ziliang Zhang – University of Bristol, Bristol, UK, e-mail: zz17635@bristol.ac.uk

Raffaele De Risi – University of Bristol, Bristol, UK, e-mail: raffaele.derisi@bristol.ac.uk

Anastasios Sextos – University of Bristol, Bristol, UK, e-mail: a.sextos@bristol.ac.uk

Abstract: This study establishes a multi-hazard probabilistic assessment procedure for assessing the integrity of monopile offshore wind turbines (OWT), considering combined loads of stochastic wind, wave, and earthquake, as well as stochastic site and structural properties. The deduced cloud-based multi-hazard fragility surface deals with the entire operational range of inflow wind speed (i.e., 3-25 m/s), from which nonnegligible probability of failure is indicated under multi-hazard excitations. It is also shown that the contribution of seismic structural demand driven by design-level earthquakes is comparable with those caused by operational-level wind and wave loads. The sensitivity of the derived fragility surfaces to a variety of statistical regression methods is scrutinised by examining the efficiency and sufficiency of alternative wind – ground motion intensity measure pairs (IM-pairs). Regression methods are comparatively assessed, and IM-pairs are provided for the purpose of assessing operating OWT multi-hazard fragility functions. The optimum IM pairs are then employed in a trained Gaussian Process Regression (GPR) scheme for cloud data regression to assess the multi-hazard fragility of the system.

Keywords: NREL 5 MW reference OWT; seismic analysis; wind – ground motion fragility

1. Introduction

In light of the rapidly growing offshore wind projects in earthquake-prone areas, the historical prospect of low seismic risks associated with offshore wind turbines (OWT) is recently re-examined. This is due to seismic-induced damages of monopile-supported OWTs that have been reported (Katsanos et al. 2016; Ali et al. 2020) and the result of theoretical studies which have highlighted the seismic vulnerability of OWTs to specific site conditions (Mardfekri et al. 2013), ground motion types or directionality (de Risi et al. 2018; Kaynia 2019; Sigurðsson et al. 2020). Contrary to some other engineering structures where each hazard can be reliably examined separately, OWTs require a multi-hazard framework due to the frequent and excessive aerodynamic and hydrodynamic loads that may be coupled with earthquake-induced forces (Zhao et al. 2019). It was found that depending on whether hazards are assessed independently (as per existing design guidelines) or jointly, significant differences in predicted OWT structural demands may arise (Valamanesh et al. 2014). Apart from the variable loads, which are of random nature, large uncertainties also manifest through stochastically distributed structural and soil properties. They complicate the problem and urge for a comprehensive understanding of structural demand and capacity using appropriate probabilistic tools. This is typically done in the form of a dual-intensity-measure (IM) fragility assessment, which results into fragility surfaces (Martin et al. 2019). It is then quite common to either assume the OWT in parked condition or to limit the considered range of inflow wind speed entirely below or above the rated wind speed (Asareh et al. 2016), to avoid the problem being entangled with OWT's blade-pitch control. The latter is a power control mechanism fitted on most modern commercial-scale wind turbines, which actively adjusts the flow-geometry of the turbine's blades to ensure safety and power efficiency. In this study, we demonstrate that multi-hazard fragility surfaces covering the OWT's entire operational range of inflow wind speed can be determined based on cloud data obtained from simplified, yet accurately calibrated, finite-element models, provided that appropriate regression methods and IM-pairs are employed. A variety of candidate regression models and IM-pairs were comparatively assessed, aiming to outline their ranked efficiency and sufficiency for assessing wind – seismic ground motion fragility functions of operating OWTs.

2. Numerical modelling

2.1. Characterisation of the site and the structure

The NREL 5 MW reference OWT (Jonkman et al. 2009) with its standard turbine, tower, transition piece and monopile geometry and material properties was used in this study (Fig. 1(a)). The seabed was situated 20.0 m deep below the mean sea level (MSL) and the monopile was embedded 36.0 m into the seabed. The turbine was assumed to operate in wind speeds ranging from 3 to 25 m/s and its rated wind speed was taken at 11.4 m/s. When the inflow wind speed is lower than the rated value, the turbine rotates at variable speed from the minimum of 6.9 rpm to the maximum of 12.1 rpm; on the other hand, when the inflow wind speed is above the rated value, the turbine is power controlled via a blade-pitching mechanism to maintain constant rotation speed and electric power output (Fig. 2). This results into a non-monotonic relationship between the inflow wind speed and the total rotor thrust exerted onto the OWT structure, as indicated in Fig. 2c. The soil profile was assumed homogenous and was characterised by nominal values of unit weight γ_{soil} = 18.0 kN/m^3, Poisson's ratio ν_{soil} = 0.25, internal friction angle φ_{soil} = 35.0 °, and pile-tip shear modulus $G_{soil,t}$ = 60,000 kPa. Structurally, Rayleigh damping ζ = 3 % was adopted (De Risi et al. 2018) for the first two lateral vibration modes of the OWT.

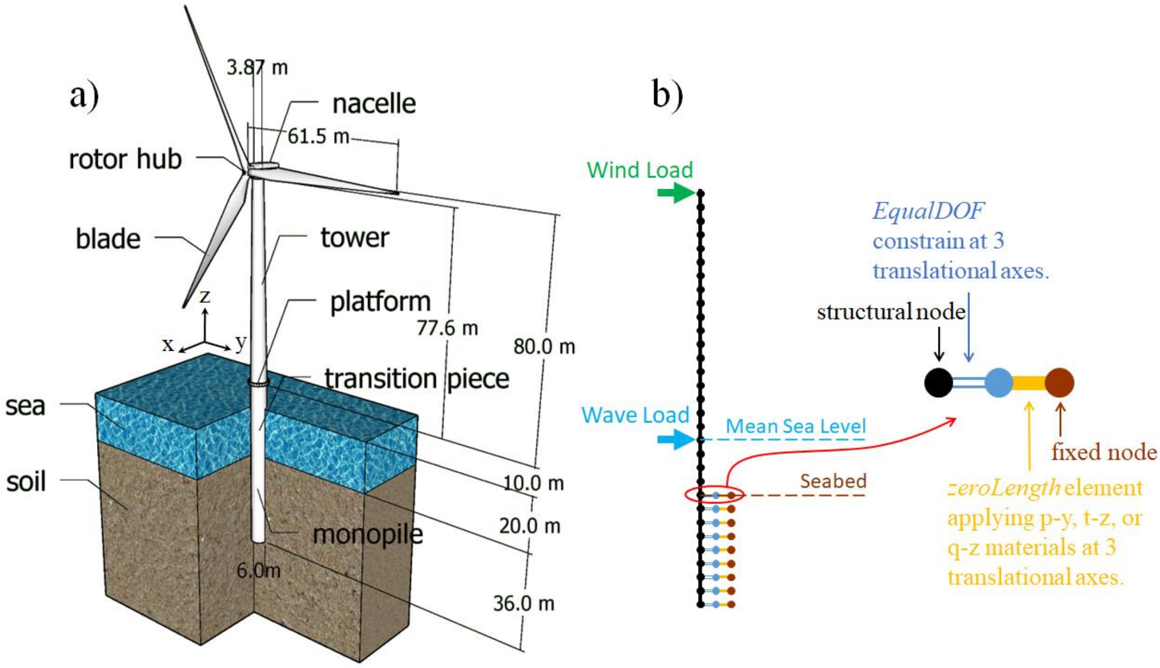

Fig. 1 – Sketch of the OWT: a) geometries, b) illustration of OpenSees models.

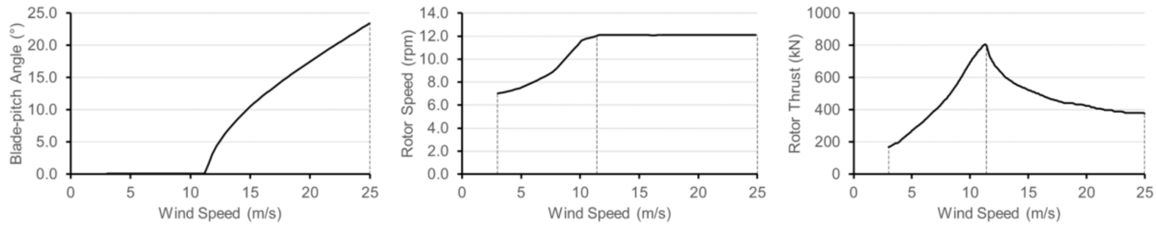

Fig. 2 – Steady-state responses of the NREL 5 MW OWT versus wind speed, (a) blade-pitch angle, (b) rotor speed, (c) rotor thrust, after (Jonkman et al. 2009).

Beam-on-nonlinear-Winkler-spring representations of the OWT (Fig. 1b) were modelled in earthquake engineering software OpenSees v3.2.0 (McKenna 2011), whilst the aero-hydro-servo-elastic simulator OpenFAST v2.3.0 (NREL 2020) was used in conjunction, to individually calibrate each wind and wave input time histories in a corresponding pair of base-fixed OWT models. This process ensured the accuracy of wind and wave inputs before they were used in the subsequent OpenSees nonlinear time history analyses. For seismic excitation, 300 earthquake records of different ground motion characteristics were selected according to a set of well-established rules (Katsanos et al. 2014) to prevent bias.

Four established engineering demand parameters (EDP) were sourced from the literature to describe failure criteria associated to two limit states. Two kinematics EDPs defined the serviceability limit state (SLS), namely the tower-top chord rotation r_{top} and the tower-top lateral acceleration a_{top}. A threshold of ±0.5 ° was prescribed for r_{top} (De Risi et al. 2018) and a threshold of 0.6 m/s^2 was prescribed for a_{top} (Ramachandran et al. 2017). The ultimate limit state (ULS) was defined by the other two stress-related EDPs, namely the Von Mises-equivalent design stress $\underline{\sigma_{eq}}$ and the Eurocode-compliant buckling-check stresses (CEN (European Committee for Standardisation, 2007), which were derived along the perimeter and the elevation of the entire OWT support-structure. The nominal yield strength of steel was taken as $f_y = 3.55\times10^5$ kPa to calculate the above two stress related EDPs. For each limit state, failure was identified when the demand to capacity ratio Y exceeded unity.

2.2. Latin Hypercube sampling of stochastic model parameters

It is known that model uncertainties have an important impact on all limit states employed to assess the performance of OWTs (Wilkie and Galasso 2020). On this account, stochastic assignment of model parameters was applied for all loads, OWT geometries, structural material properties, and soil properties. Latin Hypercube sampling (Olsson et al. 2003) was performed to generate 300 samples of near-random model parameters from a prescribed multidimensional distribution. Stochastically sampled model parameters (Fig. 3) included average wind speed V_{ave}, significant wave height H_s, representative OWT wall-thickness t, steel yield strength f_y, steel elastic modulus E_{steel}, soil unit weight γ_{soil}, soil friction angle φ_{soil}, soil shear modulus at pile-tip $G_{soil,t}$, and ground motion direction θ. The targeted probability distributions for model parameters were acquired from the literature (Ferreira and Guedes Soares 1999; Hess et al. 2002; Jones et al. 2002; Wais 2017). All randomly assigned model parameters were assumed to be uncorrelated, except for the generated mean wind speeds and significant wave heights (Fig. 4), between which a correlation coefficient of 0.85 was applied (De Flippo 2015).

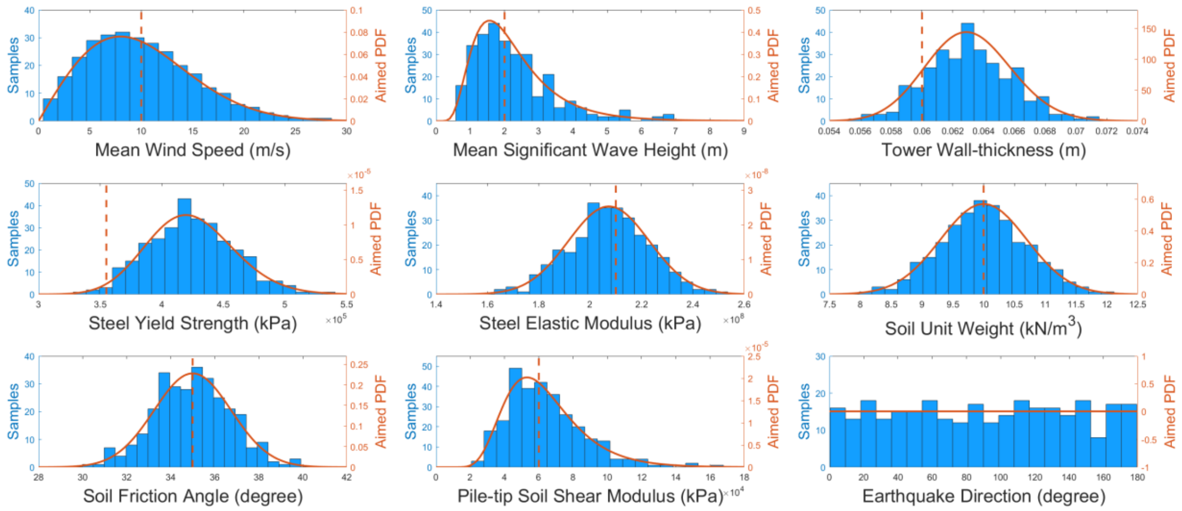

Fig. 3 – Latin hypercube sampling of the nine stochastically assigned model parameters. The orange solid curves are the targeted probability density functions (PDF), the orange dashed lines mark nominal values taken for each model parameters except for the uniformly distributed earthquake directionality, and the blue bins represent 300 generated samples.

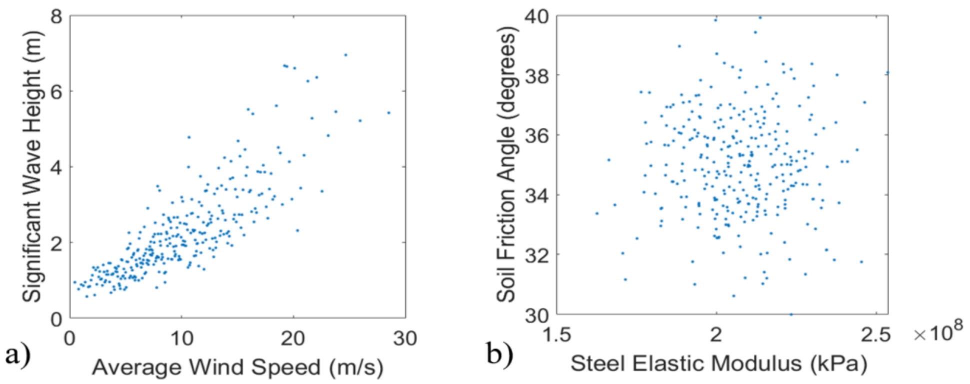

Fig. 4 – (a) Correlation between generated samples H_s and V_{ave}, and (b) an example of uncorrelated samples of φ_{soil} and E_{steel}.

3. Cloud-based multi-hazard fragility analyses

After the completion of parameter sampling and finite-element model generation, 300 nonlinear time history analyses were conducted in OpenSees to produce cloud datasets for each limit state. A multiple regression analysis was then conducted for each logarithmic transformed dataset, which consisted of one dependent variable, i.e., demand over capacity ratio, ln(Y), and two independent variables, i.e., wind and ground motion IMs, [ln(IM_{eq}), ln(IM_{wind})]. Such a regression analysis outputs estimations of conditional logarithmic mean and standard deviation across the desired range of prediction, can then be used to calculate multivariable fragility functions (Elefante et al. 2010).

3.1.1. Implementation and assessment of candidate regression models

Seven regression models were examined in this study, inlcuding linear regression (LR), 2nd to 5th order polynomial regression (PR) models, generalised linear model (GLM), and a trained Gaussian Process Regression (GPR) model. Among these models, both the LR and the GLM provide linear approximations of the relationship between 300 scalar-valued observations of Y and the vector-valued explanatory variable [IM_{eq}, IM_{wind}], whereas the PR and the GPR models are of nonlinear nature.

All regression analyses were done in MATLAB (Mathworks 2020). Key MATLAB functions for the LR and PR models include: *fit* for fitting the data to obtain LR or PR model parameters; *confint* for obtaining 95 % confidence intervals of the fitted surface; *normfit* and *makedist* for determining the value of logarithmic standard deviation; and *normcdf* for calculating the fragility function. For the GLM method, key MATLAB functions used *glmfit* for fitting the data to obtain GLM parameters and *glmval* for computing predictions given the estimated GLM parameters. Additionally, the 300 observations of demand over capacity ratio Y were transformed into categorical data which follows binomial distribution, (i.e., y = 0 indicated a safe case and y = 1indicated a failed case). For categorical data, the normal inverse cumulative distribution function, also known as the *probit* function in the context of GLM, was used as the GLM link function. For the GPR model, key MATLAB functions used include *fitrgp* for training of the model; *trainedModel.RegressionGP.Sigma* for acquiring logarithmic standard deviation of the prediction; *trainedModel.predictFcn* for acquiring logarithmic mean of the prediction; and *normcdf* for calculating the fragility function.

Efficiency of the regression models were assessed by comparing their logarithmic standard deviation $\beta_{Y|[IMeq,\, IMwind]}$ and root-mean-square error (*RMSE*) values. Visual inspection, which is of equal importance, of the cloud data fitted surfaces and the derived fragility surfaces was also performed to avoid strong underfitting or overfitting of the data.

3.1.2. Assessment of candidate IM-pairs

A variety of wind and ground motion intensity measures (IM) were assessed as combinations of IM-pairs. Candidate IMs are summarised in Table 1.

Table 1. Candidate wind (IM_{wind}) and ground motion (IM_{eq}) intensity measures.

	Type of IM	Symbol	Description
IM_{eq}	acceleration-related	PGA	peak ground acceleration
		I_a	Arias intensity
		SMA	sustained maximum acceleration
	velocity-related	PGV	peak ground velocity
		SMV	sustained maximum velocity
	displacement-related	PGD	peak ground displacement
	time-related	PGV/PGA	peak ground velocity divided by peak ground acceleration
	structure-specific	$S_a(T_1)$	spectral acceleration at the OWT's first natural period
IM_{wind}	wind-speed-related	V_{ave}	short-term average wind speed
		$V_{max.instant.}$	maximum instantaneous wind velocity
	structure-specific	$FFT_v(T_1)$	fast Fourier transform (FFT) of V_{ave} at 1st mode frequency of the OWT
		$FFT_{v,filtered}(T_1)$	Savitzky-Golay filtered $FFT_v(T_1)$

Efficiency of the IM-pairs was assessed by comparing their conditional logarithmic standard deviation $\beta_{Y|[IMeq,\, IMwind]}$ and root-mean-square error (*RMSE*) values determined using a trained GPR model. Relative sufficiency of the IM-pairs was assessed by comparing their coefficient of determination R^2 (Wang et al. 2018).

4. Results

4.1. Regression models

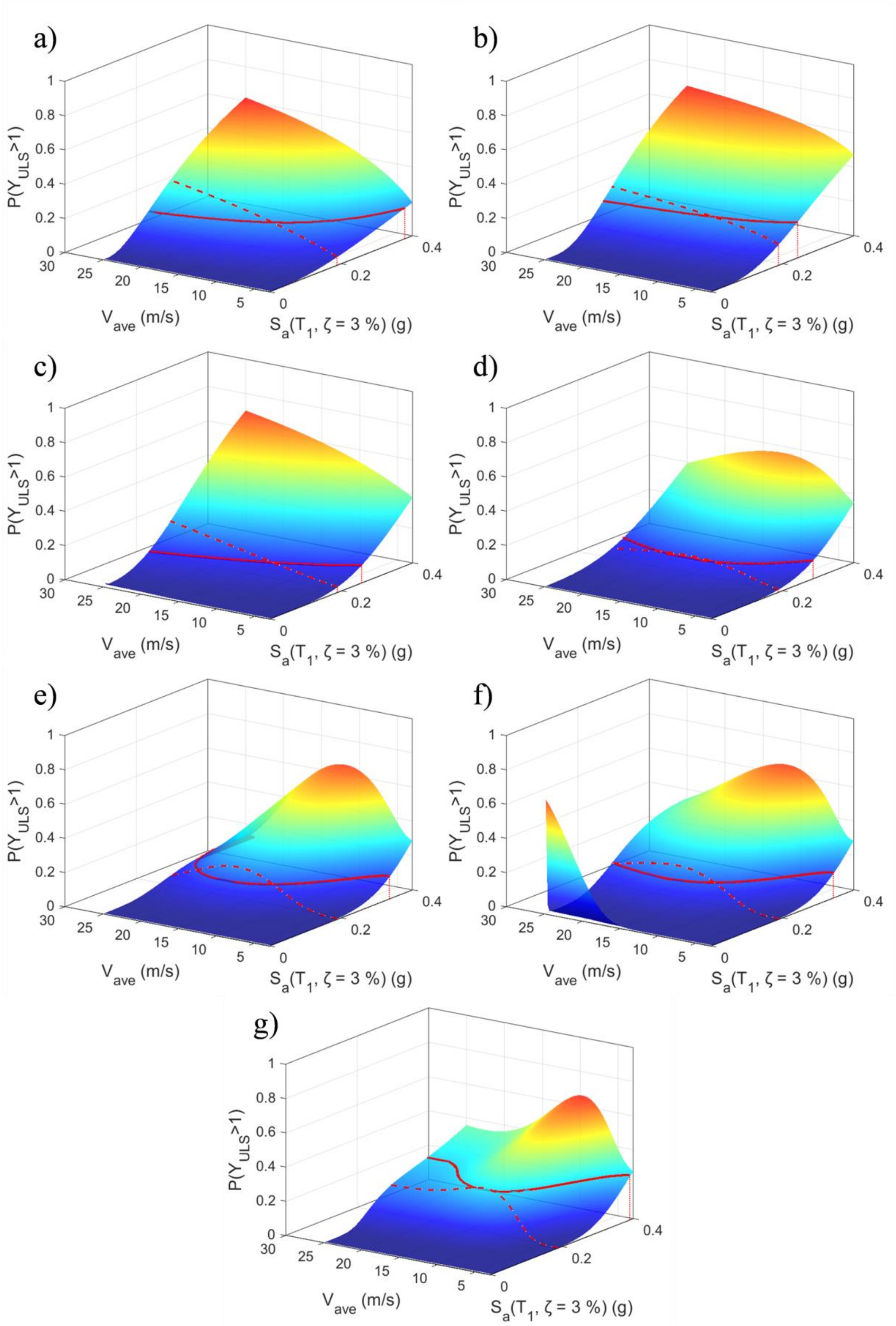

Fig. 5 – Comparison of ULS fragility surfaces computed by: (a) LR model, (b) GLM, (c)-(f) 2nd to 5th order PR models, (g) trained GPR. In each subfigure, the dashed curve marks the locations where $S_a(T_1) = S_e(T_1) = 0.189$ g, whereas the solid curve is an isopleth with $P(Y_{ULS} > 1) \equiv P(Y_{ULS} > 1|[0.189\text{ g}, 11.4\text{ m/s}])$.

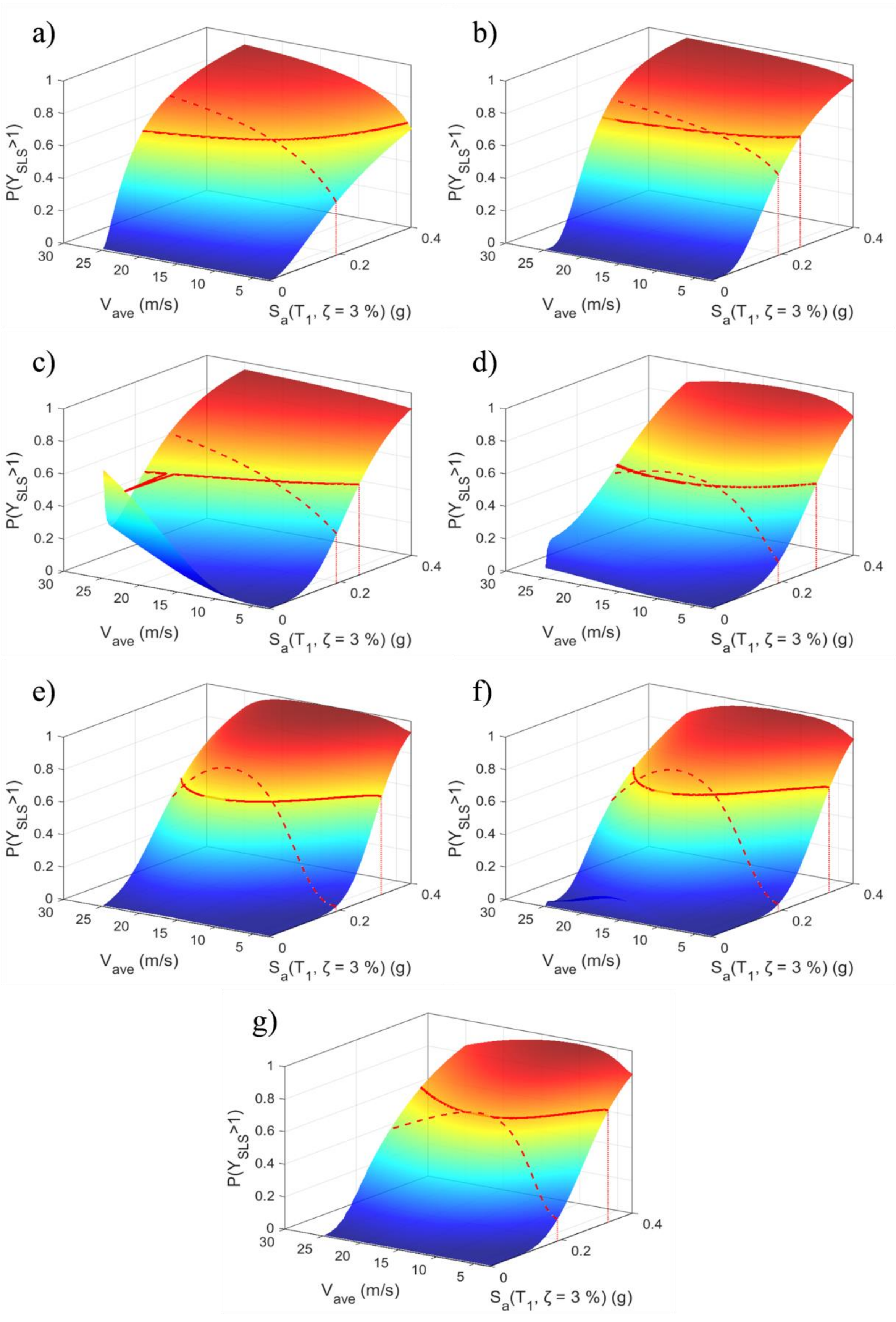

Fig. 6 – Comparison of SLS fragility surfaces computed by: (a) LR model, (b) GLM, (c) - (f) 2nd to 5th order PR model, (g) trained GPR. In each subfigure, the dashed curve marks the locations where $S_a(T_1) = S_e(T_1) = 0.189$ g, whereas the solid curve is an isopleth with $P(Y_{SLS} > 1) \equiv P(Y_{SLS} > 1|[0.189\text{ g}, 11.4\text{ m/s}])$.

Comparison of coupled wind – ground motion fragility surfaces for ULS and SLS were computed by the seven candidate regression methods as shown in Fig. 5 and Fig. 6. The LR and the GLM methods, which share the same linear principle, were found unable to adequately capture the underlying pattern from the obtained Y-[IM_{eq}, IM_{wind}] cloud data. Vastly underfitted fragility surfaces have been produced which failed to reveal the non-monotonic nature of the structural demand versus wind speed relation caused by the OWT blade-pitch control mechanism (Fig. 2c). The PR models and the GPR model, due to their nonlinear nature, were able to reflect better the trend of the data. This can be confirmed by a protuberance located along the OWT rated wind speed of 11.4 m/s, at which the total rotor thrust exserted onto the OWT tower was known to be maximised. For the PR models, however, it was noted that evident underfitting or overfitting could occur when the order of the polynomial was selected to be either too small or too large (this is also data-dependent). On the other hand, sophistication of the trained GPR model was revealed qualitatively by its ability to yield a fitted surface with the most complex shape without producing noticeable overfitting. Quantitatively, a comparison of the multi-variable logarithmic standard deviation $\beta_{Y|[IMeq, IMwind]}$ and root-mean-square error (*RMSE*) of these regression models (not applicable for GLM) confirmed the efficiency of the trained GPR model in terms of its much lower statistical dispersion (Table 2).

Additionally, two types of curves were plotted on each computed fragility surface. The dashed red curve refers the Eurocode-based design elastic spectral acceleration, $S_e(T_1)$ = 0.189 g, which was calculated assuming an anonymous site with authority-specified reference peak ground acceleration on type A ground a_{gR} = 0.5 g (CEN (European Committee for Standardisation), 2004). The solid red curve is an isopleth, on which $P(Y_{ULS} > 1) \equiv P(Y_{ULS} > 1|[0.189\text{ g}, 11.4\text{ m/s}])$, where 0.189 g is the abovementioned design spectral acceleration and 11.4 m/s is the OWT's rated operational wind speed. It can be observed that an operating OWT's probability of failure under this design-level load combination was similar to that when a feathered OWT is subjected to solely ground motion but around twice more intensive.

Table 2. Ranked recommendations of IM-pairs for operating OWT multi-hazard fragility assessment.

Index	Ranked Recommendations
$\beta_{Y\|[IMeq, IMwind]}$	GPR model > PR model (3rd order) > rest
RMSE	GPR model > PR model (4th order) > rest

4.2. IM-pairs

Relative efficiency and sufficiency rankings of wind – ground motions IM-pairs are summarised in Table 3. Note that single-IM proxies based on simple linear regressions conducted on Y-IM data pairs, which are typically used in seismic IM evaluation for ordinary civil structures, are not applicable for wind. This is because simple linear regression is inappropriate for the non-monotonically related magnitudes of OWT structural demand and operational-level wind. By assessing IM-pairs collectively using statistical indexes associated with the GPR model, which is multivariable and nonlinear, it was found that [IM_{eq}, IM_{wind}] = [PGV, V_{ave}] and [IM_{eq}, IM_{wind}] = [SMV, V_{ave}] were among the best overall performers. Moreover, the commonly used IM-pair of [IM_{eq}, IM_{wind}] = [$S_a(T_1)$, V_{ave}] was found to be not only reasonably adequate in terms of its pure efficiency and sufficiency performances, but it could also be more easily compared to code-compliant quantities such as the Eurocode 8 design elastic spectral acceleration $S_e(T_1)$, as well as many results from past studies in the literature. On the contrary, other IM-pairs were found inappropriate for assessing operating OWT multi-hazard fragility functions. The frequently used [IM_{eq}, IM_{wind}] = [PGA, V_{ave}] was found to be among the worst performers. We also noted that when the average wind speed V_{ave} was included in an IM-pair, the IM-pair's performance was often but not necessarily always better than other wind IMs in the combination, with differences that were always marginal. This is potentially due to the fact that periods with significant spectral accelerations in a typical wind spectrum are nowhere near the fundamental period of a typical monopile-supported OWT (De Risi et al. 2018). Considering the popularity of V_{ave} in the literature, not only for wind turbines but also as a legacy passed down from studies of skyscrapers or tall bridges (which, unlike operating wind turbines, are not aerodynamically controlled against wind speed), it is still considered preferable.

Table 3. Ranked recommendations of IM-pairs for operating OWT multi-hazard fragility assessment.

Index		Ranked Recommendations
efficiency	$\beta_{Y\|[IMeq, IMwind]}$	$[PGV, V_{ave}] \approx [SMV, V_{ave}] > [S_a(T_1), V_{ave}] > [PGD, V_{ave}] >$ rest
	$RMSE$	$[PGV, V_{ave}] \approx [SMV, V_{ave}] > [S_a(T_1), V_{ave}] > [I_a, V_{ave}] >$ rest
sufficiency	R^2	$[PGV, V_{ave}] \approx [SMV, V_{ave}] > [S_a(T_1), V_{ave}] > [I_a, V_{ave}] >$ rest

5. Conclusions

This study evaluates multi-hazard fragility functions for stochastically modelled operating monopile-supported OWTs. Impact of employing different statistical regression models and IM-pairs for deriving OWT multi-hazard fragility surfaces were scrutinised and the main findings are summarised below:

- OWTs are found to have non-negligible probability of exceeding SLS and ULS failing criteria under combined exposure to moderate (design-level) seismicity and wind load.
- Contrary to conclusions drawn from some of the recent studies, such as (Katsanos et al. 2017) and (Asareh et al. 2016) where "environmental" loads were significantly overpowered by earthquake forces, the present study found that the contribution of OWT structural demand driven by design-level earthquake excitations and those driven by operational-level wind and wave loads are comparable.
- The GPR model was found to be the best candidate regression method for assessing multi-hazard fragility functions of operating monopile-supported OWTs. Other nonlinear regression methods are also deemed suitable, such as a PR model with an appropriate order. Linear-based regression methods were found inappropriate in cases where the OWT's entire range of operational inflow wind speed is of interest.
- A velocity-related ground motion IM in combination with average wind speed V_{ave} makes the most efficient and sufficient IM-pair. The frequently used $[IM_{eq}, IM_{wind}]$ = $[S_a(T_1), V_{ave}]$ was found adequate in terms of IM performance, but are also desirable for its good interpretability with reference to established design codes and a vast number of published studies. The other frequently used IM-pair, $[IM_{eq}, IM_{wind}] = [PGA, V_{ave}]$, were deemed undesirable for assessing multi-hazard fragility functions of operating monopile-supported OWTs.

References

Ali A, de Risi R, Sextos A, et al (2020) Seismic vulnerability of offshore wind turbines to pulse and non-pulse records. Earthquake Engineering & Structural Dynamics 49:24–50. https://doi.org/10.1002/eqe.3222

Asareh M-A, Schonberg W, Volz J (2016) Fragility analysis of a 5-MW NREL wind turbine considering aero-elastic and seismic interaction using finite element method. Finite Elements in Analysis and Design 120:57–67. https://doi.org/10.1016/j.finel.2016.06.006

CEN (European Committee for Standardisation) (2007) Eurocode 3: Design of steel structures - Part 1-6: Strength and stability of shell structures. EN 1993-1-6: 2007 (E), Brussels

CEN (European Committee for Standardisation) (2004) Eurocode 8: Design of structures for earthquake resistance - Part 1: General rules, seismic actions and rules for buildings. EN 1998-1:2004 (E), Brussels

De Flippo M (2015) An Innovative Breakwater at Hanstholm harbour. Aalborg University

de Risi R, Bhattacharya S, Goda K (2018) Seismic performance assessment of monopile-supported offshore wind turbines using unscaled natural earthquake records. Soil Dynamics and Earthquake Engineering 109:154–172. https://doi.org/10.1016/j.soildyn.2018.03.015

De Risi R, Bhattacharya S, Goda K (2018) Seismic performance assessment of monopile-supported offshore wind turbines using unscaled natural earthquake records. Soil Dynamics and Earthquake Engineering 109:154–172. https://doi.org/10.1016/j.soildyn.2018.03.015

Elefante L, Jalayer F, Iervolino I, Manfredi G (2010) Disaggregation-based response weighting scheme for seismic risk assessment of structures. Soil Dynamics and Earthquake Engineering 30:1513–1527.

Ferreira JA, Guedes Soares C (1999) Modelling the long-term distribution of significant wave height with the Beta and Gamma models. Ocean Engineering 26:713–725.

Hess PE, Bruchman D, Assakkaf IA, Ayyub BM (2002) Uncertainties in Material and Geometric Strength and Load Variables. Naval Engineers Journal 114:139–165.

Jones A, Kramer SL, Arduino P (2002) Estimation of Uncertainty in Geotechnical Properties for Performance-Based Earthquake Engineering. PEER REPORT 2002:

Jonkman J, Butterfield S, Musial W, Scott G (2009) Definition of a 5-MW Wind Turbine Reference for Offshore System Development. Colorado, USA

Katsanos EI, Sanz AA, Georgakis CT, Thöns S (2017) Multi-hazard response analysis of a 5MW offshore wind turbine. Procedia Engineering 199:3206–3211. https://doi.org/10.1016/j.proeng.2017.09.548

Katsanos EI, Sextos AG, Elnashai AS (2014) Prediction of inelastic response periods of buildings based on intensity measures and analytical model parameters. Engineering Structures 71:161–177. https://doi.org/10.1016/j.engstruct.2014.04.007

Katsanos EI, Thons S, Georgakis C (2016) Wind turbines and seismic hazard: a state-of-the-art review. Wind Energy. https://doi.org/10.1002/we

Kaynia AM (2019) Seismic considerations in design of offshore wind turbines. Soil Dynamics and Earthquake Engineering 124:399–407. https://doi.org/10.1016/j.soildyn.2018.04.038

Mardfekri M, Gardoni P, Roesset JM (2013) Modeling Laterally Loaded Single Piles Accounting for Nonlinear Soil-Pile Interactions. Journal of Engineering 1–7. https://doi.org/10.1155/2013/243179

Martin J, Alipour A, Sarkar P (2019) Fragility surfaces for multi-hazard analysis of suspension bridges under earthquakes and microbursts. Engineering Structures 197:109169. https://doi.org/10.1016/j.engstruct.2019.05.011

Mathworks (2020) Matlab (R2020a)

McKenna F (2011) OpenSees: A Framework for Earthquake Engineering Simulation. Computing in Science & Engineering 13:58–66. https://doi.org/10.1109/MCSE.2011.66

NREL (2020) Main repository for the NREL-supported OpenFAST whole-turbine simulation code. https://github.com/OpenFAST/openfast. Accessed 30 Jul 2020

Olsson A, Sandberg G, Dahlblom O (2003) On Latin hypercube sampling for structural reliability analysis. Structural Safety 25:47–68. https://doi.org/10.1016/S0167-4730(02)00039-5

Ramachandran GK V, Vita L, Krieger A, Mueller K (2017) Design Basis for the Feasibility Evaluation of Four Different Floater Designs. Energy Procedia 137:186–195. https://doi.org/10.1016/j.egypro.2017.10.345

Sigurðsson GÖ, Rupakhety R, Rahimi SE, Olafsson S (2020) Effect of pulse-like near-fault ground motions on utility-scale land-based wind turbines. Bulletin of Earthquake Engineering 18:953–968. https://doi.org/10.1007/s10518-019-00743-9

Valamanesh V, Myers A, Hajjar J, Arwade S (2014) Probabilistic modeling of joint hurricane-induced wind and wave hazards to offshore wind farms on the Atlantic coast. In: Safety, Reliability, Risk and Life-Cycle Performance of Structures and Infrastructures. CRC Press, pp 247–252

Wais P (2017) Two and three-parameter Weibull distribution in available wind power analysis. Renewable Energy 103:15–29. https://doi.org/10.1016/j.renene.2016.10.041

Wang X, Shafieezadeh A, Ye A (2018) Optimal intensity measures for probabilistic seismic demand modeling of extended pile-shaft-supported bridges in liquefied and laterally spreading ground. Bulletin of Earthquake Engineering 16:229–257. https://doi.org/10.1007/s10518-017-0199-2

Wilkie D, Galasso C (2020) Site-specific ultimate limit state fragility of offshore wind turbines on monopile substructures. Engineering Structures 204:109903. https://doi.org/10.1016/j.engstruct.2019.109903

Zhao Z, Dai K, Camara A, et al (2019) Wind Turbine Tower Failure Modes under Seismic and Wind Loads. Journal of Performance of Constructed Facilities 33:04019015. https://doi.org/10.1061/(ASCE)CF.1943-5509.0001279